Calculation of the relativistic rise in electron-impact-excitation cross sections for highly charged ions

C. J. Bostock,[1,*] C. J. Fontes,[2,†] D. V. Fursa,[1] H. L. Zhang,[2] and Igor Bray[1]

[1]*ARC Centre for Antimatter-Matter Studies, Curtin University, GPO Box U1987, Perth, Western Australia 6845, Australia*

[2]*Computational Physics Division, Los Alamos National Laboratory, Los Alamos, New Mexico 87545, USA*

(Received 28 May 2013; published 22 July 2013)

Exact relativistic plane-wave Born (RPWB) matrix elements of the Møller interaction are incorporated in the "analytic Born subtraction technique" and employed in the relativistic convergent close-coupling method. Application to the calculation of high-energy electron-impact-excitation cross sections of highly charged hydrogenlike ions demonstrates the "Bethe rise," an effect that is manifest in Bethe's original 1932 work on relativistic high-energy, electron-impact excitation. The result represents an improvement over Bethe's relativistic high-energy theory developed in the 1930s in that (i) both target and projectile electrons are represented relativistically with Dirac spinor wave functions and (ii) the dipole approximation plus additional assumptions are not employed in the RPWB scattering amplitude of the Møller interaction.

DOI: 10.1103/PhysRevA.88.012711 PACS number(s): 34.80.Dp

I. INTRODUCTION

Recently, there has been a resurgence in the importance of the Møller interaction [or, equivalently, the generalized Breit interaction (GBI)] in bringing theory into alignment with experiment for the physics of highly charged ions. For example, this was necessary in the polarization of x rays emitted during electron-impact excitation of highly charged ions [1,2], dielectronic and radiative recombination effects [3–5], electron-impact-ionization experiments [6–8], and electron- and proton-impact excitation experiments [9]. For electron-impact excitation of highly charged hydrogenlike ions, Walker [10], Fontes *et al*. [11], and Moores and Pindzola [12] have demonstrated that the Møller interaction or GBI can increase electron-impact-excitation cross sections by up to 50% in comparison to calculations that employ only the Coulomb interaction.

In the 1930s Bethe employed the Møller interaction in a seminal paper [13] that investigated relativistic high-energy, electron-impact-excitation cross sections. Bethe employed various approximations, such as (i) the dipole approximation in the scattering amplitude, (ii) setting spinor matrix elements of Dirac $\boldsymbol{\alpha}$ matrices to $\boldsymbol{v}/c$, and (iii) capitalizing on the fact that small momentum transfer (forward scattering) dominates for high-impact energies, which allowed analytic simplification of the integrated cross-section formula. Bethe was able to produce a formula which contains the famous "Bethe rise" term, $\frac{1}{v^2}\ln(\frac{1}{1-\beta^2/c^2})$, present in electron-impact excitation, ionization, and stopping-power theory. Bethe's work formed the platform for further investigations by Møller [14], Fano [15–17], and Inokuti [18]. The latter publications all involved working in the dipole approximation. Electron-impact-ionization investigations by Scofield [19], Anholt [20], and Bote and Salvat [21] and stopping-power calculations by Cohen [22] moved beyond the dipole approximation. For electron-impact excitation, Najjari and Voitkiv [23] have recently presented relativistic distorted- and plane-wave calculations comparing equivelocity electron- versus proton-impact excitation of highly charged ions. However, similar to previous electron-impact-excitation studies [10–12] the investigation only extended to energies several threshold units (≈6) above threshold. At these low energies the Bethe rise stemming from the Møller interaction is not manifest in electron-impact-excitation cross sections for low-Z ions and is only just beginning to manifest for very highly charged ions such as U^{91+}.

Here we apply a technique, known as analytic Born subtraction, to Møller-interaction calculations that allows high-orbital-angular-momentum partial waves to be accounted for and allows us to present results to arbitrarily high energies, with the dramatic Bethe rise demonstrated for high-Z ions up to energies around 20 threshold units. The sections of this paper are organized as follows: Sec. II describes the physics underpinning the Møller interaction, Sec. III describes how the analytic Born subtraction technique can be employed with the Møller interaction, and Sec. IV contains results and discussion.

II. THE PHYSICS OF THE MØLLER INTERACTION

In 1931 Møller [24] presented a paper in which the scattering of two electrons was modeled in a relativistic manner; the electromagnetic field potential A^μ was treated classically as the Liénard-Wiechert potentials and, using correspondence principle arguments (employed by Bohr, Landau, and others at the time), incorporated the classical field in a quantum-mechanical scattering calculation. Roqué [25] and Kragh [26] provide useful historical descriptions of Møller's work. Møller worked in the Lorenz gauge (this is not a spelling error; see Lorenz's original work [27] and Bladel [28] for a discussion of the Lorenz/Lorentz confusion). Following this publication, Bethe and Fermi [29] produced one of the most fundamental papers in the history of QED, where they derived the Møller interaction from quantum electrodynamics via quantizing the electromagnetic field and treating it as a sum of harmonic oscillators. They showed that the first-order corrections to the Coulomb interaction were equivalent to the Breit interaction at low energies and the Møller interaction at both low and high energies. Thus Bethe and Fermi's expression for the interaction between two electrons, when the field A^μ mediating the interaction is quantized as a sum of harmonic oscillators, is known as the "generalized Breit interaction" [30]. Bethe and

*c.bostock@curtin.edu.au
†cjf@lanl.gov

Fermi, who worked in the Coulomb gauge, showed explicitly that their on-shell interaction matrix elements were equivalent to the Lorenz gauge matrix elements originally obtained by Møller. The gauge invariance of the matrix elements, and the importance of the on-shell case, has been studied in further detail by Hata and Grant [31]. An interesting aspect of the derivations underpinning the generalized Breit interaction presented by Bethe and Fermi [29] is that "self-interaction" terms appear in intermediate steps; Bethe and Fermi neglected these in the 1932 publication, but they were employed by Bethe 15 years later in his famous 1947 calculation of the Lamb shift in atomic hydrogen [32].

III. INCORPORATING THE MØLLER INTERACTION IN THE ANALYTIC BORN SUBTRACTION TECHNIQUE

The underlying machinery of the relativistic convergent close-coupling (RCCC) method is described in detail in [33, 34]. The analytic Born subtraction technique (or "Kummer transformation" or "top-up contribution") is described for the case of the Coulomb interaction by Fontes and Zhang [35] (see also Fursa *et al*. [34] and Sampson *et al*. [36]). The application of this technique to the Møller interaction is essentially the same as in the case of the Coulomb interaction. However, it is considerably more complicated to manipulate the exact expression for the Møller scattering amplitude into a form that can be used to calculate the corresponding cross sections due to the extra spinor algebra associated with the Dirac matrices in the Møller interaction.

The analytic Born subtraction technique works in the following way. At low energies, plane-wave Born calculations are not valid, and more accurate relativistic distorted-wave (RDW) [11], or relativistic convergent close-coupling [34], calculations are required. As the projectile energy increases, the plane-wave Born calculations become more accurate in the limit of very high energies. At intermediate and high energies and beyond, it is extremely difficult to calculate RDW or RCCC cross sections because a high-l partial-wave expansion is required in order to obtain a converged result. However, in this energy range, the individual plane-wave Born, partial-wave matrix elements also become progressively more accurate for lower and lower partial waves as the energy increases. Therefore the plane-wave Born matrix elements can be used to provide a high-angular-momentum top-up contribution to the cross sections. From a more fundamental perspective, the method is based on the fact that, for large angular momenta, the T_l matrix elements approximate the V_l matrix elements. That is, in the solution of the Lippmann-Schwinger equation, $T = V + VGT$, we can set $T_l \approx T_l^{\mathrm{B}} = V_l$, where the B superscript denotes Born. In terms of partial cross sections, $\sigma_l \approx \sigma_l^{\mathrm{B}}$, where σ_l is the partial cross section and σ_l^{B} is the relativistic plane-wave Born partial cross section. Implementation of the analytic Born subtraction technique proceeds as follows:

$$\sigma_{\mathrm{tot}} = \sum_{l=0}^{N} \sigma_l + \sum_{l=N+1}^{\infty} \sigma_l \approx \sum_{l=0}^{N} \sigma_l + \sum_{l=N+1}^{\infty} \sigma_l^{\mathrm{B}}. \qquad (1)$$

Now

$$\sigma^{\mathrm{B}} = \sum_{l=0}^{N} \sigma_l^{\mathrm{B}} + \sum_{l=N+1}^{\infty} \sigma_l^{\mathrm{B}} \Rightarrow \sum_{l=N+1}^{\infty} \sigma_l^{\mathrm{B}} = \sigma^{\mathrm{B}} - \sum_{l=0}^{N} \sigma_l^{\mathrm{B}}. \qquad (2)$$

Substituting Eq. (2) into Eq. (1), we have

$$\sigma_{\mathrm{tot}} \approx \sum_{l=0}^{N} \sigma_l + \sum_{l=N+1}^{\infty} \sigma_l^{\mathrm{B}} \approx \sum_{l=0}^{N} \sigma_l + \sigma^{\mathrm{B}} - \sum_{l=0}^{N+1} \sigma_l^{\mathrm{B}}$$
$$\approx \sum_{l=0}^{N} \left(\sigma_l - \sigma_l^{\mathrm{B}}\right) + \sigma^{\mathrm{B}}. \qquad (3)$$

This technique allows the high partial-wave ($N+1 \to \infty$) contribution to the total cross section to be accounted for by the relativistic plane-wave Born contribution. The calculation of the exact relativistic plane-wave Born (RPWB) cross section σ^{B} requires evaluation of the RPWB matrix elements of the Møller interaction. Appendix A contains the explicit evaluation of plane-wave Born matrix elements of the Møller interaction; the added complexity, compared to the Coulomb-interaction case, stems from the presence of the $\boldsymbol{\alpha} \cdot \boldsymbol{\alpha}$ term in the Møller interaction. We note that a significant amount of complexity illustrated in the Appendix was avoided by Bethe in his famous 1932 paper [13]. He employed the dipole approximation to the scattering amplitude, bypassed all the spinor algebra of the Dirac matrices (by setting $\boldsymbol{\alpha} = \boldsymbol{v}/c$ and assuming that the incident and scattered electron energies were equal), and assumed low momentum transfer (forward scattering), which allowed him to simplify the integrated cross section.

The exact Møller RPWB calculations were checked by two methods. First, the plane-wave Born cross section is the limit of the sum of the partial-wave Møller interaction cross sections ($\sigma^{\mathrm{B}} = \sum_{l=0}^{\infty} \sigma_l^{\mathrm{B}}$). Second, Najjari and Voitkiv [23] in their recent publication presented plane-wave Born results for energies up to a few ($\approx$6) threshold units above the excitation transition energy, and we could check our RPWB results against their work. Excellent agreement was found with both the first and second consistency checks.

We applied the analytic Born subtraction technique for the Møller interaction in the RCCC method to the calculation of $1s_{1/2} \to 2p_{3/2}$ electron-impact excitation of the hydrogenlike Ni^{27+}, Xe^{53+}, and U^{91+}. In Ref. [37] the QED intricacies of employing the Møller interaction (a first-order interaction) in a nonperturbative formalism are addressed. In the same work [37] it has been shown that the effects of close coupling are to introduce a series of sharp resonant peaks in the cross sections on the distorted-wave Born background. We note that it was erroneously indicated in [37] that these resonance peaks can influence effective collision strengths obtained by integrating over a Maxwellian distribution of velocities. This is not the

TABLE I. Calculated $1s_{1/2} \to 2p_{3/2}$ energy thresholds for Ni^{27+}, Xe^{53+}, and U^{91+} ions.

Target	Threshold (keV)
Ni^{27+}	8.1
Xe^{53+}	31.3
U^{91+}	102.6

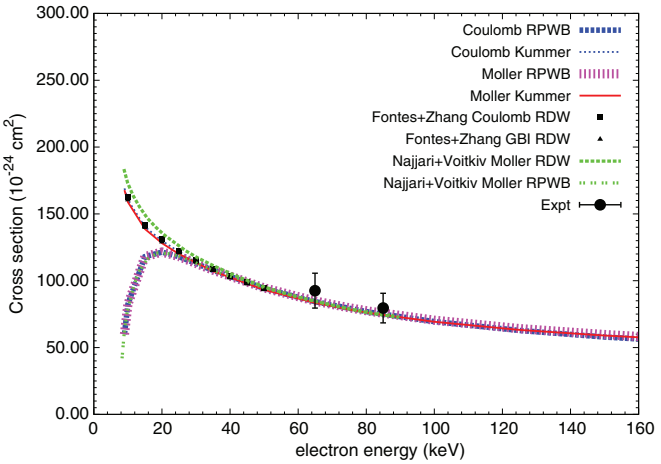

FIG. 1. (Color online) $Z = 28$ $1s_{1/2} \rightarrow 2p_{3/2}$ electron-impact-excitation cross section. Present theory is described in the text. RDW results of Fontes and Zhang are described in Ref. [40]. RDW and RPWB results of Najjari and Voitkiv are from Ref. [23]. Experiment is from Thorn *et al*. [42].

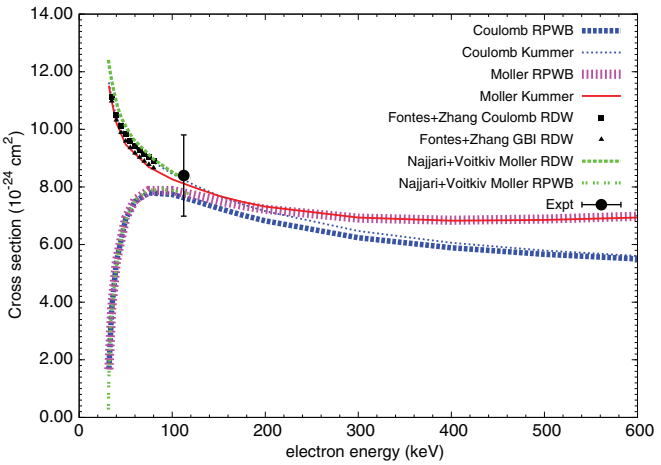

FIG. 3. (Color online) $Z = 54$ $1s_{1/2} \rightarrow 2p_{3/2}$ electron-impact-excitation cross section. Present theory is described in the text. RDW results of Fontes and Zhang are described in Ref. [40]. RDW and RPWB results of Najjari and Voitkiv are from Ref. [23]. Experiment is from Widmann *et al*. [43].

case because these resonances will be significantly radiatively damped [38,39]. Therefore in this paper we present only the background, first-order, distorted-wave Born results.

IV. RESULTS

The $1s_{1/2} \rightarrow 2p_{3/2}$ excitation thresholds for each ion species are listed in Table I. In the RCCC method, $N = 25$ partial waves were used for each ion at all energies, and then the analytic Born subtraction technique was applied to provide the high-l top-up contribution. The $1s_{1/2} \rightarrow 2p_{3/2}$ electron-impact-excitation cross section for Ni^{27+} up to 20 threshold units (160 keV) is presented in Fig. 1 . "Kummer" denotes Coulomb- or Møller-interaction results obtained with the analytic Born subtraction technique indicated by Eq. (3); that is, distorted partial waves were used up to $l = N$ and then

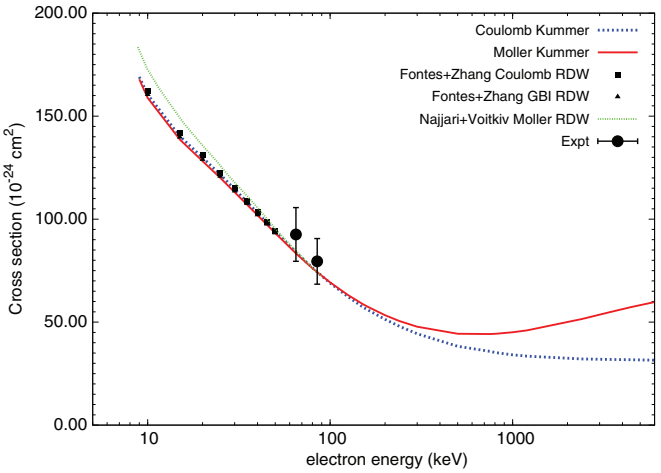

FIG. 2. (Color online) $Z = 28$ $1s_{1/2} \rightarrow 2p_{3/2}$ electron-impact-excitation cross section. Present theory is described in the text. RDW results of Fontes and Zhang are described in Ref. [40]. RDW results of Najjari and Voitkiv are from Ref. [23]. Experiment is due to Thorn *et al*. [42].

RPWB partial waves were used for $N + 1 = l \leqslant \infty$. "RPWB" denotes exact, Coulomb- or Møller-interaction RPWB results σ^B obtained by integrating the exact, analytic RPWB scattering matrix elements, as exemplified in the Appendix for the Møller interaction. These exact RPWB results essentially contain relativistic plane-wave partial waves for all possible values of l and should become progressively more accurate as the incident-electron energy increases. The results denoted "Fontes and Zhang" were computed using the Coulomb and GBI interactions in the factorized, relativistic distorted-wave approach described in [40]. We note, as described in Sec. II, that the "GBI" and "Møller" results are equivalent for the present calculations. The results denoted "Najarri and Voitkiv" are the recently published relativistic distorted-wave results of Najjari and Voitkiv [23]. These latter results are presented in order to provide a cross-check from an independent calculation and to reinforce the consistency between the methods. For the

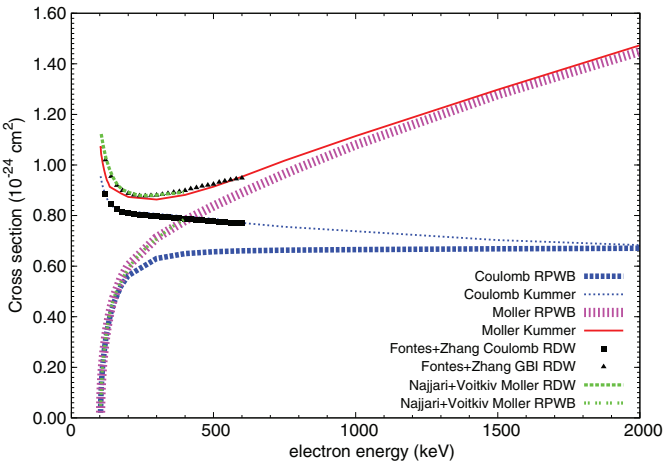

FIG. 4. (Color online) $Z = 92$ $1s_{1/2} \rightarrow 2p_{3/2}$ electron-impact-excitation cross section. Present theory is described in the text. RDW results of Fontes and Zhang are described in Ref. [40]. RDW and RPWB results of Najjari and Voitkiv are from Ref. [23].

TABLE II. Onset of the Bethe rise for $1s_{1/2} \rightarrow 2p_{3/2}$ excitation cross sections in both absolute and threshold units.

Target	Energy (keV)	Energy (u)
Ni^{27+}	600	74
Xe^{53+}	400	13
U^{91+}	250	2.5

Ni^{27+} target it was found that the Bethe rise did not manifest until the projectile energy reached approximately 600 keV. Therefore Fig. 2 shows the electron-impact-excitation cross section for higher projectile energies with a log scale on the energy axis. Note that the Bethe rise is evident in the Møller-interaction calculation but not the Coulomb-interaction calculation, which is expected to exhibit a near-constant behavior with increasing energy [41], as can be seen in Fig. 2. (The latter reference refers to electron-impact ionization, but the same concept is also valid for excitation.)

In Figs. 3 and 4 the electron-impact-excitation cross sections for Xe^{53+} and U^{91+} are presented with a linear energy scale up to 20 threshold units. The Bethe rise for the Xe^{53+} and U^{91+} targets begins at approximately 400 and 250 keV, respectively, and is most prominent for U^{91+}. We again note that in both Figs. 3 and 4, the Coulomb-interaction calculations do not exhibit a rise in the cross sections but should instead display the expected near-constant behavior at sufficiently high energies. Table II lists the energy at which the onset of the rise occurs in the Møller-interaction calculations of the $1s_{1/2} \rightarrow 2p_{3/2}$ excitation cross section for each ion. The energies are presented in both absolute units (in keV) and in threshold units, u, where the latter are dimensionless values that are obtained by dividing the impact energy by the transition energy. We note that as the Z of the target increases, the onset of the rise occurs at lower absolute projectile energies. Moreover, the onset occurs at *significantly* lower energies, when expressed in threshold units, as Z increases, which could have important consequences for the collisional-radiative modeling of high-Z plasmas.

The rise in the electron-impact-excitation cross sections remains to be confirmed by experiment. Research in this area will be of interest.

V. CONCLUSION

The exact RPWB matrix elements of the Møller interaction are incorporated in the analytic Born subtraction technique and employed in the RCCC method. Application to the calculation of high-energy electron-impact-excitation cross sections for highly charged hydrogenlike ions demonstrates the Bethe rise manifest in Bethe's original 1932 work. The main difference between the Møller RPWB matrix elements presented here and those in Bethe's 1930s work is that the exact scattering amplitude is retained in the current work, with the complete exponential and the full spinor algebra of the Dirac $\boldsymbol{\alpha}$ matrices intact, while Bethe approximated the exponential with the dipole term and set the $\boldsymbol{\alpha}$ matrix elements to $\boldsymbol{v}/c$. Further work is encouraged to determine the range of applicability of the work of Bethe [13] and Inokuti [18] with respect to target-Z range and projectile-energy range. These investigations are important in the field of high-temperature plasma modeling. It is anticipated that the Bethe rise in the high-energy region of electron-impact-excitation cross sections of highly charged hydrogenlike ions could be measured to test the accuracy of the theoretical results presented in this paper.

ACKNOWLEDGMENTS

George Csanak is thanked for discussions and translations related to this work. We are very grateful for Klaus Bartschat's *complete* German to English translation of Bethe's original paper [13] and associated discussions providing important insight into Bethe's theory. We also thank Bennaceur Najjari for providing data in electronic form. C.J.B., D.V.F., and I.B. acknowledge support from Curtin University and the Australian Research Council. The work of C.J.F. and H.L.Z. was performed under the auspices of the US Department of Energy by Los Alamos National Laboratory under Contract No. DE-AC52-06NA25396.

APPENDIX: RPWB MATRIX ELEMENTS OF THE MØLLER INTERACTION

Let $\boldsymbol{r}_1$ denote the projectile electron coordinates and $\boldsymbol{r}_2$ denote the target electron coordinates. The Møller interaction is

$$V_{12}^{\mathrm{M}} = \frac{e^2}{r_{12}}[1 - \boldsymbol{\alpha}(1)\cdot\boldsymbol{\alpha}(2)]e^{i\omega r_{12}/c}, \tag{A1}$$

where $\omega = |E_i - E_f|$ and E_i and E_f denote the initial and final kinetic energies associated with the incident and scattered electrons, respectively. The Dirac alpha matrices are

$$\boldsymbol{\alpha} = \begin{pmatrix} 0 & \boldsymbol{\sigma} \\ \boldsymbol{\sigma} & 0 \end{pmatrix}. \tag{A2}$$

The final plane-wave state of the projectile is

$$\langle \boldsymbol{r}_1 | \boldsymbol{k}_f \mu_f \rangle = \frac{1}{(2\pi)^{3/2}} V_f^{\mu_f} e^{i\boldsymbol{k}_f\cdot\boldsymbol{r}_1}, \tag{A3}$$

where

$$V_f^{\mu_f} = \sqrt{\frac{W_f + c^2}{2W_f}} \begin{pmatrix} \chi^{\mu_f} \\ \frac{c\boldsymbol{\sigma}\cdot\boldsymbol{k}_f}{W_f + c^2}\chi^{\mu_f} \end{pmatrix} \tag{A4}$$

and

$$N_f = \sqrt{\frac{W_f + c^2}{2W_f}}. \tag{A5}$$

The initial plane-wave state of the projectile is

$$\langle \boldsymbol{r}_1 | \boldsymbol{k}_i \nu_i \rangle = \frac{1}{(2\pi)^{3/2}} U_i^{\nu} e^{i\boldsymbol{k}_i\cdot\boldsymbol{r}_1}, \tag{A6}$$

where

$$U_i^{\nu} = \sqrt{\frac{W_i + c^2}{2W_i}} \begin{pmatrix} \chi^{\nu} \\ \frac{c\boldsymbol{\sigma}\cdot\boldsymbol{k}_i}{W_i + c^2}\chi^{\nu} \end{pmatrix} \tag{A7}$$

and

$$N_i = \sqrt{\frac{W_i + c^2}{2W_i}}. \tag{A8}$$

Note that $W = mc^2 + E$ is the total energy of a projectile electron and

$$\boldsymbol{\sigma}\cdot\boldsymbol{p}_f = \sigma_x p_f \sin\theta\cos\phi + \sigma_y p_f \sin\theta\sin\phi + \sigma_z p_f \cos\theta. \tag{A9}$$

As we are dealing with a spherically symmetric potential, we can set $\phi = 0$, and consequently, phase terms involving ϕ cancel in conjugate pairs, i.e., $\int \psi_f^* V \psi_i d^3r = \int \cdots e^{-im\phi} V e^{im\phi} \cdots d^3r = \int \cdots V \cdots d^3r$. Now we have

$$\boldsymbol{\sigma}\cdot\boldsymbol{p}_f = \sigma_x p_f \sin\theta + \sigma_z p_f \cos\theta \tag{A10}$$

and

$$\sigma_x \chi^\mu = \chi^{-\mu}, \quad \sigma_y \chi^\mu = 2is_\mu \chi^{-\mu}, \quad \sigma_z \chi^\mu = 2s_\mu \chi^\mu, \tag{A11}$$

where $2s_\mu = \pm 1$.

$$\sigma_x = \begin{pmatrix} 0 & 1 \\ 1 & 0 \end{pmatrix}, \quad \sigma_y = \begin{pmatrix} 0 & -i \\ i & 0 \end{pmatrix}, \quad \sigma_z = \begin{pmatrix} 1 & 0 \\ 0 & 1 \end{pmatrix}. \tag{A12}$$

Now the matrix element of the Møller interaction is

$$\begin{aligned}
&\langle\phi_f(\boldsymbol{r}_2)\boldsymbol{k}_f\mu_f|\frac{1}{r_{12}}[1-\boldsymbol{\alpha}(1)\cdot\boldsymbol{\alpha}(2)]e^{i\omega r_{12}/c}|\phi_i(\boldsymbol{r}_2)\boldsymbol{k}_i\mu_i\rangle \\
&= \langle\phi_f(\boldsymbol{r}_2)\boldsymbol{k}_f\mu_f|\frac{1}{r_{12}}e^{i\omega r_{12}/c}|\phi_i(\boldsymbol{r}_2)\boldsymbol{k}_i\mu_i\rangle \\
&\quad + \langle\phi_f(\boldsymbol{r}_2)\boldsymbol{k}_f\mu_f|\frac{-\boldsymbol{\alpha}(1)\cdot\boldsymbol{\alpha}(2)e^{i\omega r_{12}/c}}{r_{12}}|\phi_i(\boldsymbol{r}_2)\boldsymbol{k}_i\mu_i\rangle \\
&= V_{\text{term}_1} + V_{\text{term}_2}.
\end{aligned} \tag{A13}$$

Consider

$$\begin{aligned}
V_{\text{term}_1} &= \langle\phi_f|\int \frac{1}{(2\pi)^{3/2}} V_f^{\mu_f\dagger} e^{-i\boldsymbol{k}_f\cdot\boldsymbol{r}_1} \\
&\quad\times \frac{e^{i\omega r_{12}/c}}{r_{12}} \frac{1}{(2\pi)^{3/2}} U_i^{\nu_i} e^{i\boldsymbol{k}_i\cdot\boldsymbol{r}_1} d^3\boldsymbol{r}_1|\phi_i\rangle \\
&= \frac{1}{(2\pi)^3} V_f^{\mu_f\dagger} U_i^{\nu_i} \langle\phi_f|\int e^{-i\boldsymbol{k}_f\cdot\boldsymbol{r}_1} \\
&\quad\times \frac{e^{i\omega r_{12}/c}}{r_{12}} e^{i\boldsymbol{k}_i\cdot\boldsymbol{r}_1} d^3\boldsymbol{r}_1|\phi_i\rangle.
\end{aligned} \tag{A14}$$

The integral can be simplified with the Bethe trick [18]:

$$\begin{aligned}
\int e^{-i\boldsymbol{k}_f\cdot\boldsymbol{r}_1}\frac{e^{i\omega r_{12}/c}}{r_{12}}e^{i\boldsymbol{k}_i\cdot\boldsymbol{r}_1}d^3\boldsymbol{r}_1 &= \int e^{i\boldsymbol{q}\cdot\boldsymbol{r}_1}\frac{e^{i\omega r_{12}/c}}{r_{12}}d^3\boldsymbol{r}_1 \\
&= \frac{4\pi}{q^2-\omega^2/c^2}e^{i\boldsymbol{q}\cdot\boldsymbol{r}_2},
\end{aligned} \tag{A15}$$

where $\boldsymbol{q} = \boldsymbol{k}_i - \boldsymbol{k}_f$. Therefore

$$V_{\text{term}_1} = \frac{1}{(2\pi)^3} V_f^{\mu_f\dagger} U_i^{\nu_i} \frac{4\pi}{q^2-\omega^2/c^2}\langle\phi_f|e^{i\boldsymbol{q}\cdot\boldsymbol{r}_2}|\phi_i\rangle. \tag{A16}$$

Now

$$\begin{aligned}
\langle\phi_f|e^{i\boldsymbol{q}\cdot\boldsymbol{r}_2}|\phi_i\rangle &= 4\pi\sum_{\lambda\mu} Y_\mu^{\lambda*}(\hat{\boldsymbol{q}}) i^\lambda \langle R_f|j_\lambda(qr_2)|R_i\rangle \\
&\quad\times(-1)^{j_f-m_{j_f}}\begin{pmatrix} j_f & \lambda & j_i \\ -m_{j_f} & \mu & m_{j_i}\end{pmatrix} \\
&\quad\times\langle\kappa_f|\big|Y_\mu^\lambda(\hat{\boldsymbol{r}}_2)\big||\kappa_i\rangle,
\end{aligned} \tag{A17}$$

where the Wigner-Eckart theorem has been employed in the last step. Now in Eq. (A16)

$$\begin{aligned}
V_f^{\mu_f\dagger} U_i^{\nu_i} &= N_f N_i\left\{\delta_{\mu_f\nu_i} + \left(\frac{cp_f}{W_f+c^2}\right)\left(\frac{cp_i(2s_{\nu_i})}{W_i+c^2}\right)\right. \\
&\quad\left.\times\left[\sin\theta\delta_{-\mu_f\nu_i} + p_f\cos\theta(2s_{\mu_f})\delta_{\mu_f\nu_i}\right]\right\}.
\end{aligned} \tag{A18}$$

Combining Eqs. (A17) and (A18), we have

$$\begin{aligned}
V_{\text{term}_1} &= N_f N_i\left\{\delta_{\mu_f\nu_i} + \left(\frac{cp_f}{W_f+c^2}\right)\left(\frac{cp_i(2s_{\nu_i})}{W_i+c^2}\right)\right. \\
&\quad\left.\times\left[\sin\theta\delta_{-\mu_f\nu_i} + p_f\cos\theta(2s_{\mu_f})\delta_{\mu_f\nu_i}\right]\right\}\frac{4\pi}{q^2-\omega^2/c^2} \\
&\quad\times 4\pi\sum_{\lambda\mu} Y_\mu^{\lambda*}(\hat{\boldsymbol{q}}) i^\lambda \langle R_f|j_\lambda(qr_2)|R_i\rangle \\
&\quad\times(-1)^{j_f-m_{j_f}}\begin{pmatrix} j_f & \lambda & j_i \\ -m_{j_f} & \mu & m_{j_i}\end{pmatrix}\langle\kappa_f|\big|Y_\mu^\lambda(\hat{\boldsymbol{r}}_2)\big||\kappa_i\rangle.
\end{aligned} \tag{A19}$$

Note, in the above, $j = |\kappa| - 1/2$ and $l = j + \frac{|\kappa|}{2\kappa}$. We now evaluate the second term

$$V_{\text{term}_2} = \langle\phi_f(\boldsymbol{r}_2)\boldsymbol{k}_f\mu_f|\frac{-\boldsymbol{\alpha}(1)\cdot\boldsymbol{\alpha}(2)e^{i\omega r_{12}/c}}{r_{12}}|\phi_i(\boldsymbol{r}_2)\boldsymbol{k}_i\mu_i\rangle. \tag{A20}$$

Now

$$\boldsymbol{\alpha}(1)\cdot\boldsymbol{\alpha}(2) = \sum_{q'}(-1)^{q'}\alpha_{q'}^1(1)\alpha_{-q'}^1(2), \tag{A21}$$

where the spherical tensors $\alpha_{q'}^1$ are

$$\alpha_0^1 = \alpha_z \tag{A22}$$

and

$$\alpha_{\pm1}^1 = \frac{\mp(\alpha_x \pm i\alpha_y)}{\sqrt{2}}, \tag{A23}$$

so we have

$$\begin{aligned}
V_{\text{term}_2} &= \frac{-1}{(2\pi)^3}\frac{(4\pi)(4\pi)}{q^2-\omega^2/c^2}\sum_{q'}(-1)^{q'}V_f^{\mu_f\dagger}\alpha_{q'}^1(1)U_i^{\nu_i} \\
&\quad\times\sum_{\lambda\mu} i^\lambda Y_\mu^{\lambda*}(\hat{\boldsymbol{q}})\langle\phi_f|j_\lambda(qr_2)Y_\mu^\lambda(\hat{\boldsymbol{r}}_2)\alpha_{-q'}^1(2)|\phi_i\rangle.
\end{aligned} \tag{A24}$$

Now the ket $|\phi_f\rangle = |R_f j_f m_{j_f}\rangle$ becomes in position space (U denotes the upper component, and L denotes the lower)

$$\begin{pmatrix} R_U(r_2)_f\chi_{\kappa_f}^{m_{j_f}} \\ iR_L(r_2)_f\chi_{-\kappa_f}^{m_{j_f}}\end{pmatrix} \tag{A25}$$

and similarly for $|\phi_i\rangle = |R_i j_i m_{j_i}\rangle$. Using the index $\beta = +1$ and $\beta = -1$ to denote the upper and lower components, respectively, we have

$$\begin{aligned}\langle\phi_f|j_\lambda(qr_2)Y^\lambda_\mu(\hat{\boldsymbol{r}}_2)\alpha^1_{-q'}(2)|\phi_i\rangle &= \sum_\beta i^\beta \int r_2^2 dr_2 j_\lambda(qr_2)R_\beta(r_2)_f R_{-\beta}(r_2)_i \\ &\times \left\langle\kappa_f(\beta)m_{j_f}\middle|\sigma^1_{-q}(2)Y^\lambda_\mu(\hat{\boldsymbol{r}}_2)\middle|\kappa_i(-\beta)m_{j_i}\right\rangle, \end{aligned} \tag{A26}$$

where $|\kappa(\beta)m_j\rangle = |l_{\kappa(\beta)}1/2 : jm_j\rangle$ and $\beta = +1, -1$. Now

$$\begin{aligned}&\left\langle\kappa_f(\beta)m_{j_f}\middle|\sigma^1_{-q}(2)Y^\lambda_\mu(\hat{\boldsymbol{r}}_2)\middle|\kappa_i(-\beta)m_{j_i}\right\rangle \\ &= \left\langle j_f m_{j_f} : l_{\kappa_f(\beta)}1/2\middle|\sigma^1_{-q}(2)Y^\lambda_\mu(\hat{\boldsymbol{r}}_2)\middle|j_i m_{j_i} : l_{\kappa_i(\beta)}1/2\right\rangle \end{aligned} \tag{A27}$$

can be obtained by coupling $\sigma^1_{-q}(2)Y^\lambda_\mu(\hat{\boldsymbol{r}}_2)$ together as a spherical tensor as follows: first, introduce for convenience the renormalized spherical harmonic

$$Y^\lambda_\mu(\hat{\boldsymbol{r}}_2) = \sqrt{\frac{2\lambda+1}{4\pi}}C^\lambda_\mu(\hat{\boldsymbol{r}}_2). \tag{A28}$$

We have

$$\begin{aligned}\sigma^1_{-q}(2)Y^\lambda_\mu(\hat{\boldsymbol{r}}_2) &= \sigma^1_{-q}(2)\sqrt{\frac{2\lambda+1}{4\pi}}C^\lambda_\mu(\hat{\boldsymbol{r}}_2) \\ &= \sqrt{\frac{2\lambda+1}{4\pi}}\sum_{LM}[\boldsymbol{\sigma}^1\boldsymbol{C}^\lambda]^L_M C^{LM}_{1-q',\lambda\mu}, \end{aligned} \tag{A29}$$

where $C^{LM}_{1-q',\lambda\mu}$ is a Clebsch-Gordan coefficient. Now, utilizing the Wigner-Eckart theorem,

$$\begin{aligned}&\left\langle\kappa_f(\beta)m_{j_f}\middle|[\boldsymbol{\sigma}^1\boldsymbol{C}^\lambda]^L_M\middle|\kappa_i(-\beta)m_{j_i}\right\rangle \\ &= (-1)^{j_f-m_{j_f}}\begin{pmatrix} j_f & L & j_i \\ -m_{j_f} & M & m_{j_i}\end{pmatrix}\langle j_f||[\boldsymbol{\sigma}^1\boldsymbol{C}^\lambda]^L||j_i\rangle. \end{aligned} \tag{A30}$$

This can be simplified as [see Edmonds [44], Eq. (7.1.5)]

$$\begin{aligned}\langle j_f : l_f,1/2||[\boldsymbol{\sigma}^1\boldsymbol{C}^\lambda]^L||j_i : l_i,1/2\rangle &= \langle 1/2||\boldsymbol{\sigma}^1||1/2\rangle\left\langle l_{\kappa_f(\beta)}\middle||\boldsymbol{C}^\lambda||\middle|l_{\kappa_i(-\beta)}\right\rangle[(2j_f+1)(2j_i+1)(2L+1)]^{1/2} \\ &\times\begin{Bmatrix} l_{\kappa_f(\beta)} & l_{\kappa_i(-\beta)} & \lambda \\ 1/2 & 1/2 & 1 \\ j_f & j_i & L\end{Bmatrix}. \end{aligned} \tag{A31}$$

The full equation then becomes

$$\begin{aligned}V_{\text{term}_2} &= \frac{-1}{(2\pi)^3}\frac{(4\pi)(4\pi)}{q^2-\omega^2/c^2}\sum_{q'}(-1)^{q'}V_f^{\mu_f\dagger}\alpha^1_{q'}(1)U_i^{\nu_i}\sum_{\lambda\mu}i^\lambda Y^{\lambda*}_\mu(\hat{\boldsymbol{q}})\sum_\beta i^\beta\int r_2^2dr_2 j_\lambda(qr_2)R_\beta(r_2)_f R_{-\beta}(r_2)_i \\ &\times\sqrt{\frac{2\lambda+1}{4\pi}}\sum_{LM}C^{LM}_{1-q',\lambda\mu}(-1)^{j_f-m_{j_f}}\begin{pmatrix} j_f & L & j_i \\ -m_{j_f} & M & m_{j_i}\end{pmatrix}\langle 1/2||\boldsymbol{\sigma}^1||1/2\rangle\langle l_{\kappa_f(\beta)}||\boldsymbol{C}^\lambda||l_{\kappa_i(-\beta)}\rangle \\ &\times[(2j_f+1)(2j_i+1)(2L+1)]^{1/2}\begin{Bmatrix} l_{\kappa_f(\beta)} & l_{\kappa_i(-\beta)} & \lambda \\ 1/2 & 1/2 & 1 \\ j_f & j_i & L\end{Bmatrix}, \end{aligned} \tag{A32}$$

where

$$\langle 1/2||\boldsymbol{\sigma}^1||1/2\rangle = \sqrt{6} \tag{A33}$$

and

$$\left\langle l_{\kappa_f(\beta)}\middle||\boldsymbol{C}^\lambda||\middle|l_{\kappa_i(-\beta)}\right\rangle = (-1)^{l_{\kappa_f(\beta)}}\left[\left(2l_{\kappa_f(\beta)}+1\right)\left(2l_{\kappa_i(-\beta)}+1\right)\right]^{1/2}\begin{pmatrix} l_{\kappa_f(\beta)} & \lambda & l_{\kappa_i(-\beta)} \\ 0 & 0 & 0\end{pmatrix}. \tag{A34}$$

The spinor matrix elements of the Dirac matrices (as spherical tensors) are

$$V_f^{\mu_f\dagger}\alpha^1_{q'}(1)U_i^{\nu_i} = N_f N_i\left(\frac{\chi^{\mu_f\dagger}cp_i\left(2s_{\nu_i}\right)}{W_i+c^2}+\frac{\left\{cp_f[\sin\theta\chi^{-\mu_f}+\cos\theta\left(2s_{\mu_f}\right)]\chi^{\mu_f}\right\}^\dagger}{W_f+c^2}\right)\sigma^1_{q'}\chi^{\nu_i}. \tag{A35}$$

For $\sigma^1_{q'}\chi^{\nu_i}$ we have

$$\begin{aligned}q' = -1 &\Rightarrow \sigma^1_{-1}\chi^{\nu_i} = \frac{(\sigma_x-i\sigma_y)\chi^{\nu_i}}{\sqrt{2}} = \frac{\left(\chi^{-\nu_i}-i2is_{\nu_i}\chi^{-\nu_i}\right)}{\sqrt{2}} = \frac{\left(1+2s_{\nu_i}\right)\chi^{-\nu_i}}{\sqrt{2}}, \\ q' = 1 &\Rightarrow \sigma^1_1\chi^{\nu_i} = \frac{-(\sigma_x+i\sigma_y)\chi^{\nu_i}}{\sqrt{2}} = \frac{-\left(\chi^{-\nu_i}+i2is_{\nu_i}\chi^{-\nu_i}\right)}{\sqrt{2}} = \frac{-\left(1-2s_{\nu_i}\right)\chi^{-\nu_i}}{\sqrt{2}}, \\ q' = 0 &\Rightarrow \sigma^1_0\chi^{\nu_i} = \sigma_z\chi^{\nu_i} = 2s_{\nu_i}\chi^{\nu_i}. \end{aligned} \tag{A36}$$

Therefore the total interaction is

$$V_{12}^{\mathrm{M}} = V_{\mathrm{term}_1} + V_{\mathrm{term}_2} = \frac{-1}{(2\pi)^3}\frac{(4\pi)(4\pi)}{q^2-\omega^2/c^2}\sum_{q'}(-1)^{q'}V_f^{\mu_f\dagger}\alpha_{q'}^1(1)U_i^{\nu_i}\sum_{\lambda\mu} i^\lambda Y_\mu^{\lambda*}(\hat{\boldsymbol{q}})\langle\phi_f|j_\lambda(qr_2)Y_\mu^\lambda(\hat{\boldsymbol{r}}_2)\alpha_{-q'}^1(2)|\phi_i\rangle$$
$$+\frac{-1}{(2\pi)^3}\frac{(4\pi)(4\pi)}{q^2-\omega^2/c^2}\sum_{q'}(-1)^{q'}V_f^{\mu_f\dagger}\alpha_{q'}^1(1)U_i^{\nu_i}\sum_{\lambda\mu} i^\lambda Y_\mu^{\lambda*}(\hat{\boldsymbol{q}})\sum_\beta i^\beta\int r_2^2 dr_2 j_\lambda(qr_2)R_\beta(r_2)_f R_{-\beta}(r_2)_i$$
$$\times\sqrt{\frac{2\lambda+1}{4\pi}}\sum_{LM}C^{LM}_{1-q',\lambda\mu}(-1)^{j_f-m_{j_f}}\begin{pmatrix} j_f & L & j_i\\ -m_{j_f} & M & m_{j_i}\end{pmatrix}\langle j_f|\langle 1/2||\boldsymbol{\sigma}^1||1/2\rangle\langle l_{\kappa_f(\beta)}||\boldsymbol{C}^\lambda||l_{\kappa_i(-\beta)}\rangle$$
$$\times[(2j_f+1)(2j_i+1)(2L+1)]^{1/2}\begin{Bmatrix} l_{\kappa_f(\beta)} & l_{\kappa_i(-\beta)} & \lambda\\ 1/2 & 1/2 & 1\\ j_f & j_i & L\end{Bmatrix}, \tag{A37}$$

with insertion of Eqs. (A33), (A34), and (A35) for $\langle l_{\kappa_f(\beta)}||\boldsymbol{C}^\lambda||l_{\kappa_i(-\beta)}\rangle$, $\langle 1/2||\boldsymbol{\sigma}^1||1/2\rangle$, and $V_f^{\mu_f\dagger}\alpha_{q'}^1(1)U_i^{\nu_i}$, respectively.

[1] C. J. Bostock, D. V. Fursa, and I. Bray, Phys. Rev. A **80**, 052708 (2009).
[2] C. J. Bostock, D. V. Fursa, and I. Bray, Can. J. Phys. **89**, 503 (2011).
[3] N. Nakamura, A. P. Kavanagh, H. Watanabe, H. A. Sakaue, Y. Li, D. Kato, F. J. Currell, and S. Ohtani, Phys. Rev. Lett. **100**, 073203 (2008).
[4] S. Fritzsche, A. Surzhykov, and T. Stöhlker, Phys. Rev. Lett. **103**, 113001 (2009).
[5] Z. Hu, X. Han, Y. Li, D. Kato, X. Tong, and N. Nakamura, Phys. Rev. Lett. **108**, 073002 (2012).
[6] R. E. Marrs, S. R. Elliott, and D. A. Knapp, Phys. Rev. Lett. **72**, 4082 (1994).
[7] D. L. Moores and K. J. Reed, Phys. Rev. A **51**, R9 (1995).
[8] C. J. Fontes, D. H. Sampson, and H. L. Zhang, Phys. Rev. A **51**, R12 (1995).
[9] A. Gumberidze, D. B. Thorn, C. J. Fontes, B. Najjari, H. L. Zhang, A. Surzhykov, A. Voitkiv, S. Fritzsche, D. Banaś, H. Beyer *et al.*, Phys. Rev. Lett. **110**, 213201 (2013).
[10] D. W. Walker, J. Phys. B **8**, 760 (1975).
[11] C. J. Fontes, D. H. Sampson, and H. L. Zhang, Phys. Rev. A **47**, 1009 (1993).
[12] D. L. Moores and M. S. Pindzola, J. Phys. B **25**, 4581 (1992).
[13] H. Bethe, Z. Phys. **76**, 293 (1932).
[14] C. Møller, Ann. Phys. (Berlin, Ger.) **14**, 531 (1932).
[15] U. Fano, Phys. Rev. **95**, 1198 (1954).
[16] U. Fano, Phys. Rev. **102**, 385 (1956).
[17] U. Fano, Annu. Rev. Nucl. Sci. **13**, 1 (1963).
[18] M. Inokuti, Rev. Mod. Phys. **43**, 297 (1971).
[19] J. H. Scofield, Phys. Rev. A **18**, 963 (1978).
[20] R. Anholt, Phys. Rev. A **19**, 1004 (1979).
[21] D. Bote and F. Salvat, Phys. Rev. A **77**, 042701 (2008).
[22] S. M. Cohen, Phys. Rev. A **68**, 012720 (2003).
[23] B. Najjari and A. B. Voitkiv, Phys. Rev. A **87**, 034701 (2013).
[24] C. Møller, Z. Phys. **70**, 786 (1931).
[25] X. Roqué, Arch. Hist. Exact Sci. **44**, 197 (1992).
[26] H. Kragh, Arch. Hist. Exact Sci. **43**, 299 (1992).
[27] L. Lorenz, Philos. Mag. **34**, 287 (1867).
[28] J. Bladel, IEEE Antennas Propag. Mag. **33**, 69 (1991).
[29] H. Bethe and E. Fermi, Z. Phys. **77**, 296 (1932).
[30] J. B. Mann and W. R. Johnson, Phys. Rev. A **4**, 41 (1971).
[31] J. Hata and I. P. Grant, J. Phys. B **17**, L107 (1984).
[32] H. A. Bethe, Phys. Rev. **72**, 339 (1947).
[33] C. J. Bostock, J. Phys. B **44**, 083001 (2011).
[34] D. V. Fursa, C. J. Bostock, and I. Bray, Phys. Rev. A **80**, 022717 (2009).
[35] C. J. Fontes and H. L. Zhang, Phys. Rev. A **76**, 040703(R) (2007).
[36] D. H. Sampson, H. L. Zhang, and C. J. Fontes, Phys. Rep. **477**, 111 (2009).
[37] C. J. Bostock, D. V. Fursa, and I. Bray, Phys. Rev. A **86**, 042709 (2012).
[38] T. W. Gorczyca and N. R. Badnell, J. Phys. B **29**, L283 (1996).
[39] H. L. Zhang and A. K. Pradhan, J. Phys. B **28**, L285 (1995).
[40] C. J. Fontes, D. H. Sampson, and H. L. Zhang, Phys. Rev. A **49**, 3704 (1994).
[41] C. J. Fontes, D. H. Sampson, and H. L. Zhang, Phys. Rev. A **59**, 1329 (1999).
[42] D. B. Thorn, P. Beiersdorfer, G. V. Brown, R. L. Kelley, C. A. Kilbourne, and F. S. Porter, J. Phys. Conf. Ser. **163**, 012036 (2009).
[43] K. Widmann, P. Beiersdorfer, G. V. Brown, J. R. C. Lopez-Urrutia, A. L. Osterheld, K. J. Reed, J. H. Scofield, and S. B. Utter, AIP Conf. Proc. **506**, 44 (2000).
[44] A. R. Edmonds, *Angular Momentum in Quantum Mechanics* (Princeton University Press, Princeton, NJ, 1957).